Structural Deformation and Displacement of a Disc Winding due to Standard Switching Impulse Voltage via Finite Element Method

Nurul Farahwahida Md Yasid[1], Norhafiz Azis[1,2]*, Jasronita Jasni[1], Mohd Fairouz Mohd Yousof[3], Mohd Aizam Talib[4] and Avinash Srikanta Murthy[5]

[1]*Advanced Lightning, Power and Energy Research Centre (ALPER), Faculty of Engineering, Universiti Putra Malaysia, 43400 UPM, Serdang, Selangor, Malaysia*
[2]*Institute of Nanoscience and Nanotechnology (ION2), Universiti Putra Malaysia, 43400 UPM, Serdang, Selangor, Malaysia*
[3]*Faculty of Electrical and Electronics Engineering, Universiti Tun Hussein Onn Malaysia, 86400 Parit Raja, Johor, Malaysia*
[4]*TNB Labs Sdn. Bhd, Kajang, Selangor, 43000, Malaysia*
[5]*Transformer Technology Centre, Hitachi Energy, 390013, India*

ABSTRACT

Switching operations in a power system network can lead to transient overvoltage in the high voltage (HV) winding of distribution transformers that causes high-stress build-up. This paper presents the relationship between electromagnetic force due to a standard switching impulse (SSI) and mechanical deformation/displacement behaviours for a disc-type transformer. The analysis was carried out based on a three-dimensional (3D) modelling of a continuous HV disc winding configuration whereby it is subjected to the switching transient voltage and force excitations through the finite element method (FEM). The electric transient solver analysed the static and dynamic aspects of the electromagnetic forces associated with the variation of forces versus time. The transient structural solver evaluated the structural behaviours of the disc winding related to the axial height and radial width of the winding under electromagnetic forces. It is found that the positively dominant axial force generated in the winding with a magnitude of 8.7 N causes the top and bottom layers of disc winding to tilt and displace. In addition, the positive average radial force of 1.4 N causes the circumference of the winding to experience hoop tension and outwardly stretch.

Keywords: Disc winding, electromagnetic forces, structural behaviours, switching transient, transformer

Nurul Farahwahida Md Yasid, Norhafiz Azis, Jasronita Jasni, Mohd Fairouz Mohd Yousof,
Mohd Aizam Talib and Avinash Srikanta Murthy

INTRODUCTION

According to a global survey conducted by CIGRE WG A2.37, among the major contributors to transformer failures is the winding, including deformation cases (Tenbohlen et al., 2016; Tenbohlen et al., 2017). The winding deformations normally occur at locations between spacers and barriers (Kojima et al., 1980). These phenomena are usually caused by the high electromagnetic forces from the overvoltage/overcurrent in the power system networks (Da Costa Oliveira Rocha et al., 2014). The majority of transformer insulation failures and abnormal electromagnetic stresses on windings are caused by repetitive in-service switching operations (Agrawal, 2001b; Yasid et al., 2023; Yutthagowith, 2022).

The primary fundamental of switching transient is the interruption of the steady state of a power system network caused by the switching operations. High resonance overvoltage can occur once the oscillations of the switching operations match with the resonance of a transformer (Bjerkan, 2005). It can trigger overvoltage up to 4 or 5 times higher than the normal power frequency, resulting in a steep-fronted surge that generates large stress in a transformer (Bhuyan & Chatterjee, 2015). This condition can also occur once the transient voltage excitation wave frequencies are close to the major frequencies of the transformer (Massaro & Antunes, 2009). Surge arresters are normally installed as surge and overvoltage protection devices but are only sensitive to voltage amplitudes. Therefore, the incoming transient voltage wave might still cause resonance behaviours in the winding even when the amplitude is well below the protection level if there is a matching in the frequencies (Agrawal, 2001a; Florkowski et al., 2020).

The finite element method (FEM) is known as one of the best alternative methods to solve engineering problems, and it can provide results closer to physical phenomena (Rao et al., 2012; Rao, 2005; Yan et al., 2016). Several studies have been conducted to examine the magnetic fields, stresses and electromagnetic forces during transient conditions through the FEM. The electromagnetic forces on the transformer windings based on FEM are carried out in Arivamudhan and Santhi (2019), Dawood et al. (2019), Faiz et al. (2011) and Fonseca et al. (2016). The axial and radial forces are found to be the highest at the end and middle sections of the windings, respectively. Other studies focus on the stress concentration factors (Hodhigere et al., 2018; Muminovic et al., 2015). It is found that the irregularities in the stress distributions cause abnormal stress concentration on the winding. The previous study also examined the magnetic fields within transformers of different geometrical dimensions and magnetic parameters (Hussein & Hameed, 2022). It has been discovered that different winding configurations can affect the magnetic field and electromagnetic force distributions. In addition, the leakage flux induced by different types of faults can affect the structural deformation and displacement of the windings (Fonseca et al., 2018; Nazari, 2013; Zhang et al., 2021).

It is known that the structural displacements and deformations of windings can lead to mechanical faults. It can be divided into two main modes, which are axial displacement and radial deformation (Bagheri et al., 2012; Gutten et al., 2011; Nurmanova et al., 2019; Ou et al., 2022; Tahir & Tenbohlen, 2019). Axial displacement can cause a complete winding displacement, tilting and bending of the windings. Radial deformation causes hoop tension , forced and free buckling. When both forces are excessive, it can cause spiralling and telescoping of windings. These conditions challenge manufacturers and users to compute the changes in the structural behaviours of different winding configurations and faults since generic condition interpretation could not be applied. Furthermore, limited analysis that focuses on the disc winding configuration is available. This winding type is common in a core-type transformer but is more complex than the spiral-type winding (van Jaarsveld, 2013).

The findings of this study have significant implications for characterising the behaviours of the electromagnetic forces as well as identifying the corresponding deformation and displacement behaviours of a disc winding structure due to a switching transient. The study presents a case study of a single-phase HV winding model of a 30 MVA disc-type distribution transformer. A 3D model that considers 8-disc winding is simulated through Ansys. The electromagnetic forces and mechanical deformation/ displacement due to standard switching impulse (SSI) are investigated through electric transient and transient structural analyses. The stress concentration with characteristics of deformation and displacement of the disc winding obtained from this study are anticipated to provide helpful insight for physical configurations at the design phase of the transformer winding.

METHODS

Design and Disc Winding Modelling

In order to evaluate the structural performance of the disc winding design, the solution strategy began with the evaluation of the numerical electric transient due to the switching transient. The geometrical winding model was constructed based on the structural parameters and material properties of a 33/11 kV, 30 MVA disc-type transformer, as shown in Tables 1 and 2. Figure 1 shows the single-phase front cross-

Table 1

The HV winding geometrical specifications of Dyn11, 30 MVA disc-type transformer

Parameters	Specification
Number of discs in one phase	96
Number of turns per disc	30
Height of conductor	11.5 mm
Width of the conductor	2.4 mm
The thickness of the insulation (double-sided)	0.5 mm
Distance between each disc	3 mm
Cooling duct between layers 12 and 13	5 mm
Inner radius of the HV winding	374.5 mm
Outer radius of the HV winding	466.5 mm
Total circumference of the HV winding	79.17 mm
Height of HV winding	1437 mm
Insulation between HV – LV windings	20 mm

Table 2
Winding and mechanical properties used in FEM

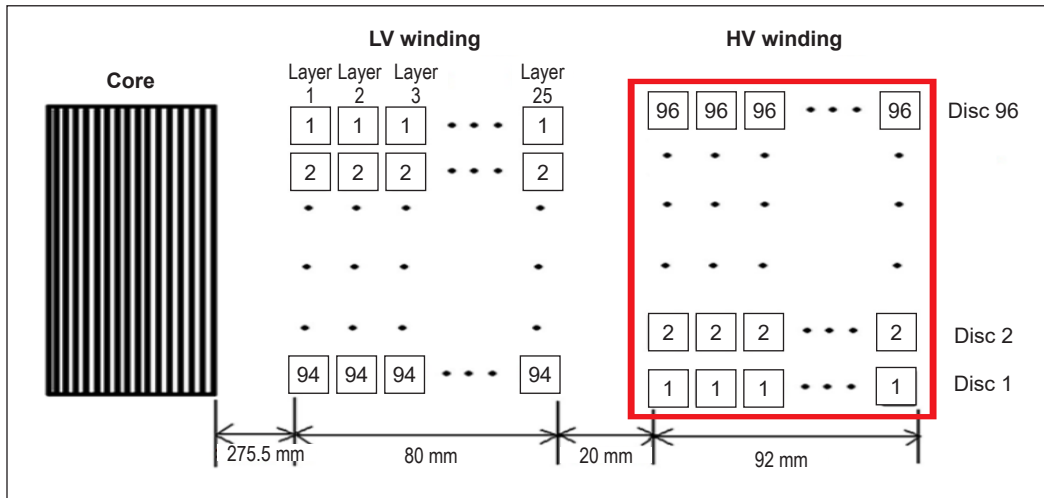| Part	Materials	Density (kg m^{-3})	ME (GPa)	PR
Conductor	Copper	7850	113	0.3
Insulation	Kraft paper	930	1.1	0.001
Fixed support	Steel	7850	200	0.3

Figure 1. Single-phase 33/11 kV transformer front cross-section view

section view of the transformer winding. In this case, only HV winding was modelled and analysed since the electromagnetic forces induced by the excitation inrush mainly acted on this side (Zhang et al., 2021). It is known that the transient condition causes the transformer's core to oversaturate, leading to reduced permeability (van Jaarsveld, 2013). Therefore, the core was not considered during transient analysis. The spacers are not considered in the electrical and mechanical analyses since it is not electrically active and is not subjected to significant mechanical loads.

The 3D geometric model of the disc winding that includes conductors, insulation materials and winding fixed supports can be seen in Figure 2. Figure 2(a) shows the perspective view, and Figure 2(b) shows the ¼ symmetrical top and trimetric views of the model. The model consists of continuous 8 discs, each comprising 6 conductors and 5 turns. Due to the nature of the transformer's symmetrical structure, the 3D geometric model was split into 4 symmetrical parts. This symmetry boundary condition setting leads to efficient computational in terms of space and run times.

In this study, the winding modelling was simplified and considered an ideal model focused only on the 8 topmost discs. An implicit assumption was made that the winding was a rotation symmetric cylinder with a continuous arrangement of the copper conductors. The
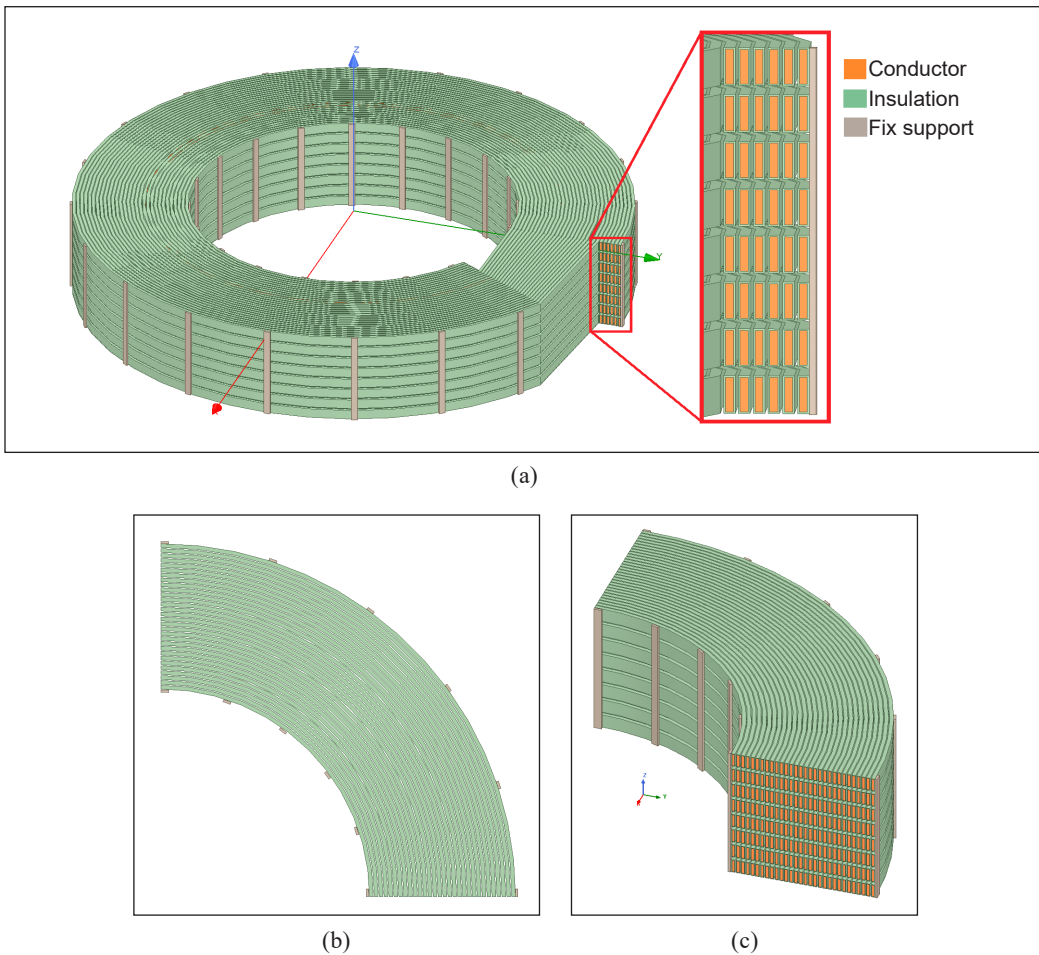
(a)

(b)   (c)

Figure 2. Details of HV disc winding model: (a) Perspective view; and (b) ¼ symmetrical top and trimetric view

structure presents the geometry, material properties, capacitive and inductive couplings for every element of the disc winding. The skin effect was also considered. The winding fixed supports were placed at the inner and outer layers of the winding to simulate clamping. The 3D geometric model was subjected to a mesh of free tetrahedrons network composed of 492 active bodies, 2,678,899 nodes and 1,271,896 elements.

The current simulation work was performed based on a similar approach to Murthy et al. (2020), whereby the 3D geometric model validation was conducted by comparing the results of simulated and measured frequency response analyses (FRA). The study showed good agreement between simulated and measured FRAs, which indicated that the winding model was adequate and applicable to this analysis. Another study showed that the parameters of the winding model were near the actual transformer once good agreement was found between the simulated and measured FRAs (Behjat & Mahvi, 2015).

Standard Switching Impulse Voltage Distribution

The SSI voltage as per IEC 60071-1, 2019 and IEEE Std C37.30, 2018, defined the front and tail times as 250 and 2500 µs. The impulse generator circuit generated the SSI voltage waveform (Ren et al., 2016). In total, 1 cycle of SSI voltage was used as the input data for the force analysis. The voltage was defined in per unit (p.u) based on the ratio of the peak overvoltage to the peak phase-to-earth voltage for the transformer winding. For this case, the analysis considered the highest magnitude of a switching surge that could be achieved,

Figure 3. The overall scheme of switching impulse analysis

which was 5 p.u, equivalent to 165 kV. This SSI voltage was superimposed on each disc windings to determine the total electromagnetic force. Figure 3 shows the overall scheme of the SSI voltage application on the winding.
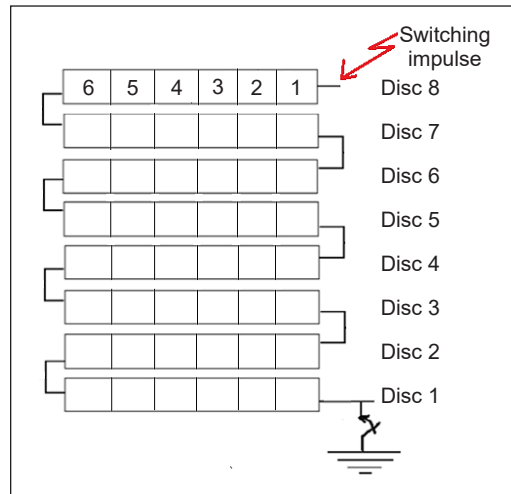
Relationship of Electromagnetic Forces and Winding Displacement/Deformation

The computed electromagnetic forces from the electric transient analysis were transferred to the transient structural analysis to obtain the deformation/displacements of the winding. The winding model was remodelled using the Space Claim in the Ansys Workbench to certify its initial structure. The internal overvoltage was obtained as a result of the response within the winding due to the 1 cycle of SSI voltage. The transient current and leakage flux generated the electromagnetic forces in the winding. The forces in the winding can be obtained by the Lorentz force, as shown in Equation 1.

$$d\vec{F} = id\vec{l} \times \vec{B} \tag{1}$$

Where F is the force, I is the current density, and B is the flux density. The magnetic computation of the 3D modelling was described in x, y and z planes since the current was normal to those planes (Feyzi & Sabahi, 2008). The component of leakage flux density can be expressed as vector potential, as seen in Equation 2 (Ahn et al., 2012).

$$B_x = -\frac{\partial A_\phi}{\partial_z}, \qquad B_y = 0, \qquad B_z = \frac{1}{r}\frac{\partial r A_\phi}{\partial_x} \tag{2}$$

Where B_x, B_y and B_z are directional components of leakage flux density, and A_ϕ is the magnetic vector potential. The electromagnetic force on the winding was expressed using

the Lorentz force as per Equations 3 and 4 (Ahn et al., 2011).

$$F = \int_V J_y \hat{y} \times (B_x \hat{x} + B_z \hat{z}) dv = F_x \hat{x} + F_z \hat{z} \qquad [3]$$

$$F_x = B_z \times J_y, \quad F_z = B_x \times J_y \qquad [4]$$

Where, J_y is the y-directional current density, $\hat{x}$, $\hat{y}$ and $\hat{z}$ are the unit vectors in the winding plane. When the winding was subjected to a high electromagnetic force, the winding deformation or displacement could be initiated. The deformation can be defined by elastic-plastic deformation, stress and strain control (Zhang et al., 2014). The relation between stress and mass force in space can be described based on Equation 5.

$$\begin{cases} \dfrac{\partial \sigma_r}{\partial r} + \dfrac{\partial \tau_{zr}}{\partial z} + \dfrac{\sigma_r - \sigma_\theta}{r} + f_r = 0 \\ \dfrac{\partial \sigma_z}{\partial z} + \dfrac{\partial \tau_{rz}}{\partial r} + \dfrac{\tau_{rz}}{r} + f_z = 0 \end{cases} \qquad [5]$$

Where f_r and f_z are the radial and axial forces exerted on the winding. σ_r, σ_θ and σ_z are the radial, tangential and axial stress. The relationship between strain and displacement describes the displacement. The strain-displacement describes how the applied forces on the winding cause it to deform and result in displacement of the winding. The strain displacement can be expressed by Equation 6.

$$\begin{cases} \varepsilon_r = \dfrac{\partial u_r}{\partial r} \qquad\qquad\qquad \varepsilon_\theta = \dfrac{u_r}{r} \\ \varepsilon_z = \dfrac{\partial u_z}{\partial z} \qquad\qquad \gamma_{rz} = \dfrac{\partial u_r}{\partial z} + \dfrac{\partial u_z}{\partial r} \end{cases} \qquad [6]$$

Where ε_r, ε_θ, and ε_z are the radial strain, tangential and axial strain, γ_{zr} is the shear strain, u_r and u_z are the radial and axial displacements. The relationship between stress and strain in space can be expressed by Equation 7.

$$\begin{cases} \varepsilon_r = \dfrac{1}{E}[\sigma_r - \mu(\sigma_\theta + \sigma_z)] \qquad \varepsilon_\theta = \dfrac{1}{E}[\sigma_\theta - \mu(\sigma_z + \sigma_r)] \\ \varepsilon_z = \dfrac{1}{E}[\sigma_z - \mu(\sigma_r + \sigma_\theta)] \qquad\qquad \gamma_{zr} = \dfrac{2(1+\mu)}{E}\mathcal{T}_{zr} \end{cases} \qquad [7]$$

Where $\mathcal{T}_{zr}$ is the shear stress, μ is the Poisson ratio of the winding material, and E is the elastic modulus according to the mechanical properties of the winding material.

RESULTS AND DISCUSSIONS

The deformations were classified into two modes: which are directional and total deformations. Directional deformation refers to the deformation of the disc winding

structure in a particular defined direction known as the *x*-, *y*- and *z*-directions. These defined directions were correlated to the expressed electromagnetic force directions. The total deformation is the vector sum of all the directional deformations. It should be noted that the forces generated from 1 cycle of SSI would not cause the winding to deform/displace. In this case, the scale of deformations was increased to analyse the possible deformation and displacement on the disc winding.

Electromagnetic Force Generated Due to the SSI

The electromagnetic forces generated due to 1 cycle of the SSI are displayed in the time domain, as seen in Figure 4. The forces are given into 3 directional components as the 3D model planes, *x*-, *y*- and *z*-directions. The *x*- and *y*-directional forces represent the radial force, while the *z*-directional force represents the axial force. It is found that both *y*- and *z*-directional forces increase while the *x*-directional force decreases after 1500 μs. The peak amplitude of the *x*-, *y*- and *z*-directional forces is -0.5 N, 3.2 N, and 8.7 N, respectively. The average radially *x*- and *y*-directional force on the winding is 1.4 N, a positively directed force. This condition indicates that the width of the disc winding experiences a horizontal tensile force. The axially *z*-directional force is positively directed, which signifies that vertical tensile force is projected along the height of the disc winding. The axial force in the disc winding is observed to be more dominant than the radial force.
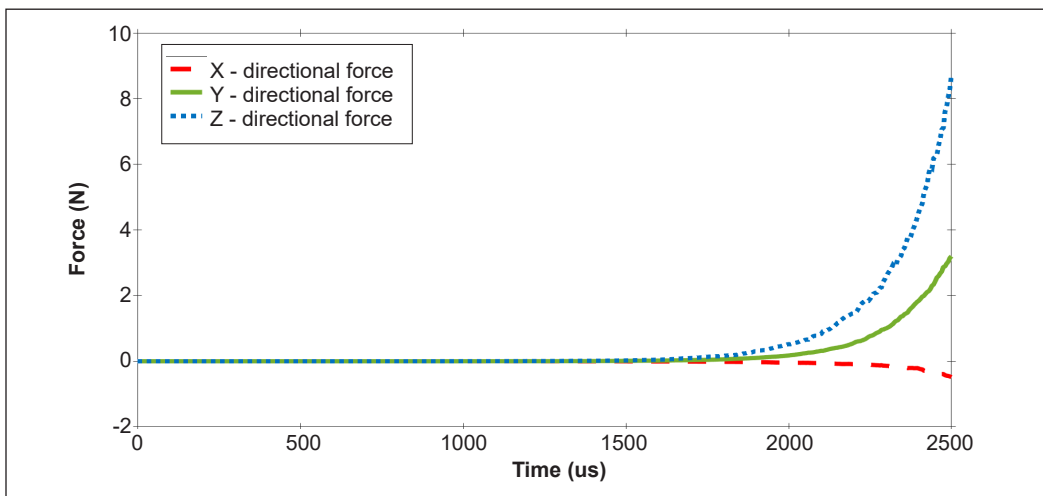

Figure 4. The electromagnetic forces generated due to 1 cycle of SSI

Directional Deformations

The variations of winding structural behaviours along the *x*-, *y*- and *z*-directions over 1 cycle of SSI waveform with 0.5× deformation scale factor are shown in Tables 3 and 4. The average *x*-, *y*- and *z*-directional deformations are concentrated at *x* = 0, *y* = 0, and *z* =
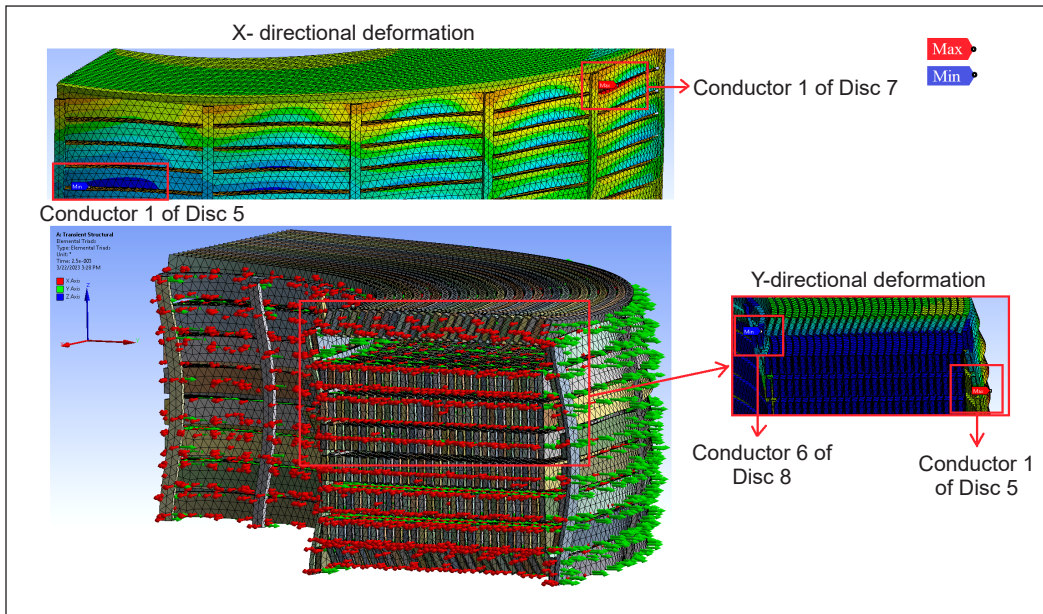
Table 3
Results of directional deformations of disc winding

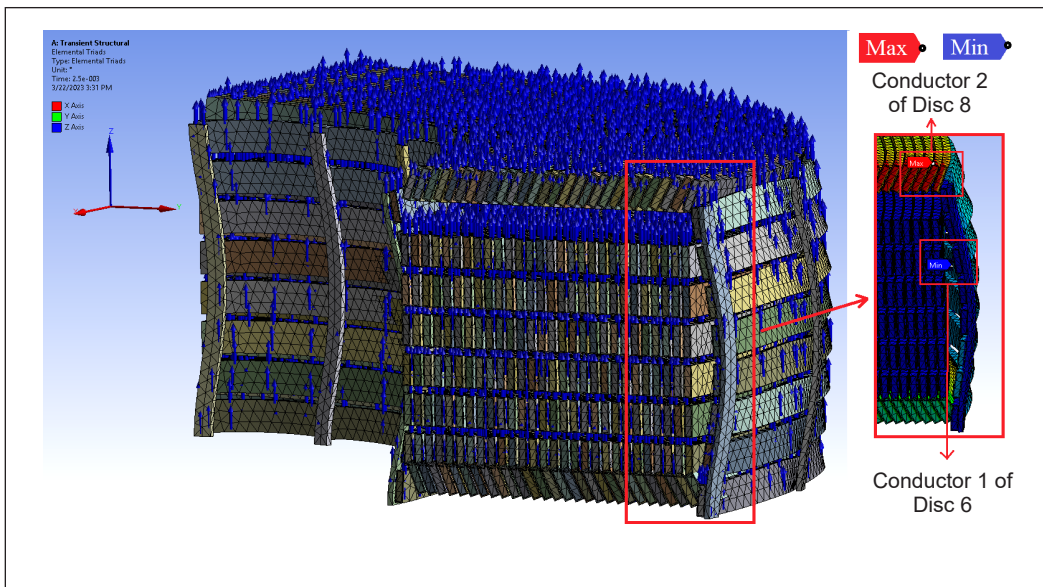| Directional deformation	Minimum (mm)	Maximum (mm)	Average (mm)	Minimum Occurs On	Maximum Occurs On
X	-1.24×10^{-5}	2.97×10^{-6}	-7.22×10^{-7}	Conductor 1 (Disc 5)	Conductor 1 (Disc 7)
Y	-1.22×10^{-6}	3.51×10^{-5}	3.12×10^{-6}	Conductor 6 (Disc 8)	Conductor 1 (Disc 5)
Z	-2.56×10^{-6}	3.81×10^{-5}	6.11×10^{-6}	Conductor 1 (Disc 6)	Conductor 2 (Disc 8)

0 planes (Ahn et al., 2011). The directional deformations are presented with the element triads that show the directions of the deformation moments.

The directional deformation analysis of the disc winding shows that the maximum deformation occurs in the *z*-direction, which is along the axial height of the winding. The highest deformation is located on the topmost disc layer with a peak magnitude of 3.81×10^{-5} mm. This deformation is about 6 times higher than the average deformation of this direction. The axial displacements are obvious at the top and bottom layers of the disc winding, as seen in Figure 5. The winding experiences axial displacement and tilting of conductors. The positive *z*-directional deformation causes the bottom and top disc layers to displace slightly upward from their original position. In addition, it is observed that the conductors at both disc layers tilt to the right and left directions at a small angle ranging between 5° and 10°. In this case, the support structures seem to bend or not evenly align since they are experiencing deformations. It causes the axial force to be imposed unevenly on the winding, which leads to different degrees of tilting in different disc layers. These results align with the findings of Behjat et al. (2018) and Dawood et al. (2020), whereby higher axial forces are detected at the end discs and cause the tilt of conductors.

The second highest deformation occurs at the outer-most winding or circumference of the winding, which is in the *y*-direction with a peak magnitude of 3.51×10^{-5} mm. The *y*-directional deformation acts perpendicularly to the axis of the disc winding, causing the hoop tension. This hoop tension refers to the tensile stress that occurs perpendicularly to the winding axis. This stress leads to the stretch of the winding conductor along the circumference of the winding, which results in changes in its dimension and shape. The outer layers of the winding conductors bend outwardly between each fixed support as the fixed support structure has higher stiffness than the winding conductors, as seen in Figure 5. On the other hand, the *x*-directional deformation is quite small, with a peak magnitude of 2.97×10^{-6} mm and results in insignificant structural deformation. These results match those observed in earlier studies by Behjat et al. (2018) and Meng and Wang (2004), which found that radial forces act outward on the outer winding. Based on the overall results of the directional deformation analysis, it is observed that the deformation is higher in the axial direction as compared to the radial direction.

(a)

(b)

Figure 5. Directional deformations of disc winding at: (a) x- and y-directions; and (b) z-direction

Total Deformation

The variation of total deformation that shows the total structural behaviours of the disc winding over 1 cycle of SSI with a 0.5× deformation scale factor is shown in Table 4 and Figure 6.

Table 4
Results of the total deformation of disc winding

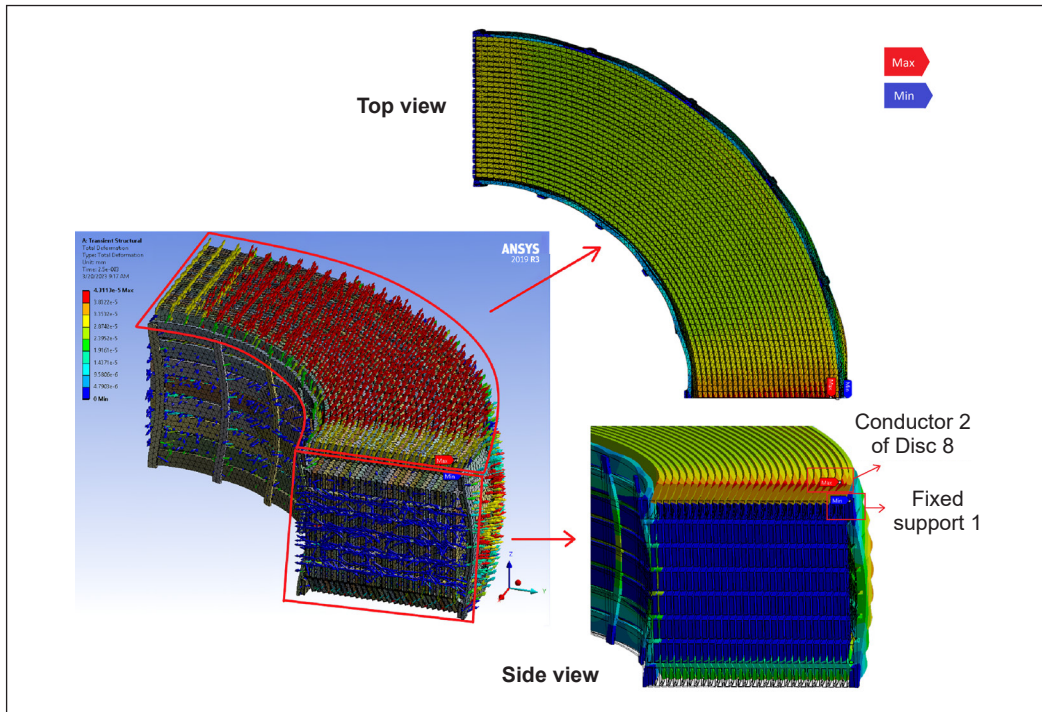| Total deformation	Minimum (mm)	Maximum (mm)	Average (mm)	Minimum Occurs On	Maximum Occurs On
	0	4.31×10^{-5}	7.30×10^{-6}	Fixed support 1	Conductor 2 (Disc 8)

Figure 6. Total deformation of disc winding due to SSI

The total deformation analysis shows that the maximum deformation occurs on the conductor at the topmost disc layer of the winding, with a peak magnitude of 4.31×10^{-5} mm. The minimum deformation occurs on the fixed supports, with 0 mm. The deformations at the fixed support sections are lower than those of the winding conductors. Radial deformations are more obvious at the middle sections of the winding and uniform across the width of the winding. The deformation in the axial direction is obvious at the top and bottom disc windings. The analysis also reveals that deformation is the highest at the outer-most layer of the winding, in both radial and axial directions. It is because the sections with higher leakage flux experience higher electromagnetic forces and are prone to experience deformation and displacement (Faiz et al., 2011). The deformation and displacement computation results show that along the z-direction, the axial force gradually increases from the middle to the end of the HV windings. Along the x and y directions, the radial force linearly increases from the inner to outer sides of the HV winding.

CONCLUSION

This work examines the electromagnetic force and structural deformation/displacement characteristics of a disc winding. The axial force generated in the winding causes the top and bottom layers of disc winding to tilt and displace with a peak magnitude of 3.81×10^{-5} mm. The radial force causes the circumference of the winding to experience hoop tension and outwardly stretch with an average magnitude of 1.9×10^{-5} mm. The deformation and displacement are more likely to occur to the outer layer of the disc winding, whether in axial or radial directions. The disc winding experiences a higher axial force; therefore, axial structural displacement is more dominant as compared to radial structural deformation. These findings generally strengthen the finding that high-stress concentration can lead to a high degree of deformation and displacement of windings. In the case of disc winding subjected to the SSI, consideration should be given to the design of the winding conductors and its axial clamping system or fixed supports to ensure the disc winding structural integrity.

ACKNOWLEDGEMENTS

REFERENCES

Agrawal, K. C. (2001a). Surge arresters: Application and selection. In *Industrial Power Engineering Handbook* (Vol. 18, pp. 681-719). Butterworth-Heinemann. https://doi.org/10.1016/b978-075067351-8/50096-9

Agrawal, K. C. (2001b). Voltage surges - Causes, effects and remedies. In *Industrial Power Engineering Handbook* (Vol. 17, pp. 555-585). Butterworth-Heinemann. https://doi.org/10.1016/b978-075067351-8/50095-7

Ahn, H. M., Lee, J. Y., Kim, J. K., Oh, Y. H., Jung, S. Y., & Hahn, S. C. (2011). Finite-element analysis of short-circuit electromagnetic force in power transformer. *IEEE Transactions on Industry Applications, 47*(3), 1267-1272. https://doi.org/10.1109/TIA.2011.2126031

Ahn, H. M., Oh, Y. H., Kim, J. K., Song, J. S., & Hahn, S. C. (2012). Experimental verification and finite element analysis of short-circuit electromagnetic force for dry-type transformer. *IEEE Transactions on Magnetics, 48*(2), 819-822. https://doi.org/10.1109/TMAG.2011.2174212

Arivamudhan, M., & Santhi, S. (2019). Analysis of Mechanical integrity in power transformer using statistical techniques. In *2019 IEEE International Conference on Electrical, Computer and Communication Technologies (ICECCT)* (pp. 1-6). IEEE Publishing. https://doi.org/10.1109/ICECCT.2019.8869152

Bagheri, M., Naderi, M., & Blackburn, T. (2012). Advanced transformer winding deformation diagnosis: Moving from off-line to on-line. *IEEE Transactions on Dielectrics and Electrical Insulation, 19*(6), 1860-1870. https://doi.org/10.1109/TDEI.2012.6396941

Behjat, V., & Mahvi, M. (2015). Statistical approach for interpretation of power transformers frequency response analysis results. *IET Science, Measurement and Technology, 9*(3), 367-375. https://doi.org/10.1049/iet-smt.2014.0097

Behjat, V., Shams, A., & Tamjidi, V. (2018). Characterization of power transformer electromagnetic forces affected by winding faults. *Journal of Operation and Automation in Power Engineering, 6*(1), 40-49. https://doi.org/10.22098/joape.2018.2436.1210

Bhuyan, K., & Chatterjee, S. (2015). Electric stresses on transformer winding insulation under standard and non-standard impulse voltages. *Electric Power Systems Research, 123*, 40-47. https://doi.org/10.1016/j.epsr.2015.01.019

Bjerkan, E. (2005). High frequency modeling of power transformers - Stresses and Diagnostic (Doctoral dissertation). Norwegian University of Science and Technology, Norway. https://ntnuopen.ntnu.no/ntnu-xmlui/handle/11250/256420

Da Costa Oliveira Rocha, A., Holdyk, A., Gustavsen, B., van Jaarsveld, B. J. Portillo, A., Badrazadeh, B., Roy, C., & Rahimpour, E. (2014). *Electrical Transient Interaction Between Transformer and the Power System, Part-2: Case studies*. CIGRE. https://e-cigre.org/publication/577B-electrical-transient-interaction-between-transformers-and-the-power-system-part-2-case-studies

Dawood, K., Komurgoz, G., & Isik, F. (2019). Computation of the axial and radial forces in the windings of the power transformer. In *2019 4th International Conference on Power Electronics and their Applications (ICPEA)* (pp. 1-6). IEEE Publishing. https://doi.org/10.1109/ICPEA1.2019.8911132

Dawood, K., Komurgoz, G., & Isik, F. (2020). Investigating the effect of axial displacement of transformer winding on the electromagnetic forces. In *2020 7th International Conference on Electrical and Electronics Engineering (ICEEE)* (pp. 360-364). IEEE Publishing. https://doi.org/10.1109/ICEEE49618.2020.9102472

Faiz, J., Ebrahimi, B. M., & Abu-Elhaija, W. (2011). Computation of static and dynamic axial and radial forces on power transformer windings due to inrush and short circuit currents. In *2011 IEEE Jordan Conference on Applied Electrical Engineering and Computing Technologies (AEECT)* (pp. 1-8). IEEE Publishing. https://doi.org/10.1109/AEECT.2011.6132487

Feyzi, M. R., & Sabahi, M. (2008). Finite element analyses of short circuit forces in power transformers with asymmetric conditions. In *2008 IEEE International Symposium on Industrial Electronics* (pp. 576-581). IEEE. https://doi.org/10.1109/ISIE.2008.4677272

Florkowski, M., Furgał, J., & Kuniewski, M. (2020). Propagation of overvoltages in the form of impulse, chopped and oscillating waveforms in transformer windings - Time and frequency domain approach. *Energies, 13*(2), 1-17. https://doi.org/10.3390/en13020304

Fonseca, W., Lima, D., Lima, A., Soeiro, N. S., & Nunes, M. V. A. (2016). Analysis of electromagnetic-mechanical stresses on the winding of a transformer under inrush currents conditions. *International Journal of Applied Electromagnetics and Mechanics, 50*(4), 511-524. https://doi.org/10.3233/JAE-150044

Fonseca, W. S., Lima, D. S., Lima, A. K. F., Nunes, M. V. A., Bezerra, U. H., & Soeiro, N. S. (2018). Analysis of structural behavior of transformer's winding under inrush current conditions. *IEEE Transactions on Industry Applications, 54*(3), 2285-2294. https://doi.org/10.1109/TIA.2018.2808273

Gutten, M., Ik, J. J. U. R. Č., Brandt, M., & Polansky, R. (2011). Mechanical effects of short-circuit currents analysis on autotransformer windings. *Electrical Engineering, 87*(7), 272-275. http://pe.org.pl/articles/2011/7/62.pdf

Hodhigere, Y., S Jha, J., Tewari, A., & Mishra, S. (2018). Finite element analysis-based approach for stress concentration factor calculation. In *Proceedings of Fatigue, Durability and Fracture Mechanics* (pp. 1-6). Springer. https://doi.org/10.1007/978-981-10-6002-1

Hussein, W. J., & Hameed, K. R. (2022). Finite-element calculation of electromagnetic forces in the deferent shapes of distribution transformers winding under short circuit condition. *Journal of Engineering and Sustainable Development, 26*(3), 44-61. https://doi.org/10.31272/jeasd.26.3.6

Kojima, H., Miyata, H., Shida, S., & Okuyama, K. (1980). Buckling strength analysis of large power transformer winding subjected to electromagnetic force under short circuit. *IEEE Transactions on Power Apparatus and Systems, PAS-99*(3), 1288-1297. https://doi.org/10.1109/TPAS.1980.319761

Massaro, U., & Antunes, R. (2009). Electrical transient interaction between transformers and power system - Brazilian experience. *International Conference on Power Systems Transients (IPST2009), Kyoto, Japan, 3*(6), 1-9. http://www.ipst.org/techpapers/2009/papers/257.pdf

Meng, Z., & Wang, Z. (2004). The analysis of mechanical strength of HV winding using finite element method, part I calculation of electromagnetic forces. In *39th International Universities Power Engineering Conference* (UPEC) (Vol. 1, pp. 170-174). IEEE Publishing.

Muminovic, A. J., Saric, I., & Repcic, N. (2015). Numerical analysis of stress concentration factors. *Procedia Engineering, 100*, 707-713. https://doi.org/10.1016/j.proeng.2015.01.423

Murthy, A. S., Azis, N., Jasni, J., Othman, M. L., Yousof, M. F. M., & Talib, M. A. (2020). Extraction of winding parameters for 33 / 11 kV , 30 MVA transformer based on finite element method for frequency response modelling. *PLOS ONE, 15*(8), Article e0236409. https://doi.org/10.1371/journal.pone.0236409

Nazari, A. (2013). Leakage fluxes and mechanical forces calculation on the single phase shell- type transformer winding under over currents by 2-D and 3-D finite element methods. *Journal of Electrical Engineering, 13*(4), 1-8.

Nurmanova, V., Bagheri, M., Zollanvari, A., Aliakhmet, K., Akhmetov, Y., & Gharehpetian, G. B. (2019). A new transformer FRA measurement technique to reach smart interpretation for inter-disk faults. *IEEE Transactions on Power Delivery, 34*(4), 1508-1519. https://doi.org/10.1109/TPWRD.2019.2909144

Ou, Q., Luo, L., Li, Y., Lin, Y., & Tian, Y. (2022). A dynamic relative displacement evaluation method for extra-high voltage transformer withstanding short-circuit impact. *IET Generation, Transmission & Distribution, 17*(6), 1310-1320. https://doi.org/10.1049/gtd2.12736

Rao, M. A., Khanna, M. R., Somaiya, K. J., & Gangopadhyay, M. (2012). Applications of finite elements method (FEM) - An overview. *International Conference on Mathematical Sciences, 28*(31), 1-8. https://doi.org/10.13140/RG.2.2.36294.42565

Rao, S. S. (2005). Overview of finite element method. In *The Finite Element Method in Engineering* (pp. 3-45). Elsevier. https://doi.org/10.1016/B978-0-7506-7828-5.X5000-8

Ren, M., Zhang, C., Dong, M., Ye, R., & Albarracín, R. (2016). A new switching impulse generator based on transformer boosting and insulated gate bipolar transistor trigger control. *Energies, 9*(644), 1-15. https://doi.org/10.3390/en9080644

Tahir, M., & Tenbohlen, S. (2019). A comprehensive analysis of windings electrical and mechanical faults using a high-frequency model. *Energies, 13*(1), Article 105. https://doi.org/10.3390/en13010105

Tenbohlen, S., Jagers, J., & Vahidi, F. (2017). Standardized survey of transformer reliability: On behalf of CIGRE WG A2.37. In *2017 International Symposium on Electrical Insulating Materials (ISEIM)* (Vol. 2, pp. 593-596). IEEE Publishing. https://doi.org/10.23919/ISEIM.2017.8166559

Tenbohlen, S., Vahidi, F., & Jagers, J. (2016). A worldwide transformer reliability survey. In *VDE High Voltage Technology 2016; ETG-Symposium* (pp. 1-6). VDE. https://ieeexplore.ieee.org/document/7776092

van Jaarsveld, B. J. (2013). *Wide Band Modelling of An Air-Core Power Transformer Winding* (Master dissertation). Stellenbosch University, South Africa. http://scholar.sun.ac.za/handle/10019.1/85823

Yan, X., Yu, X., Shen, M., Xie, D., Bai, B., & Wang, Y. (2016). Calculation of stray losses in power transformer structural parts using finite element method combined with analytical method. In *2015 18th International Conference on Electrical Machines and Systems (ICEMS)* (pp. 320-324). IEEE Publishing. https://doi.org/10.1109/ICEMS.2015.7385051

Yasid, N. F. M., Azis, N., Yousof, M. F. M., Jasni, J., Talib, M. A., & Murthy, A. S. (2023). Electromagnetic force distribution computations due to switching surge in disc-type winding. *Indonesian Journal of Electrical Engineering and Computer Science, 30*(2), 659-669. https://doi.org/10.11591/ijeecs.v30.i2.pp659-669

Yutthagowith, P. (2022). An accurate evaluation of switching impulse voltages for high-voltage tests. *Energies, 15*(4760), 1-10. https://doi.org/https://doi.org/10.3390/en15134760

Zhang, C., Ge, W., Xie, Y. I., & Li, Y. (2021). Comprehensive Analysis of winding electromagnetic force and deformation during no-load closing and short-circuiting of power transformers. *IEEE Access, 9*, 73335-73345. https://doi.org/10.1109/ACCESS.2021.3068054

Zhang, H., Yang, B., Xu, W., Wang, S., Wang, G., Huangfu, Y., & Zhang, J. (2014). Dynamic deformation analysis of power transformer windings in short-circuit fault by FEM. *IEEE Transactions on Applied Superconductivity, 24*(3), 5-8. https://doi.org/10.1109/TASC.2013.2285335